Available online at www.sciencedirect.com
ScienceDirect
Journal of the European Ceramic Society 32 (2012) 1359–1364
www.elsevier.com/locate/jeurceramsoc

Origins of colour in Yb–Si–Al–O–N glasses

Wynette Redington *, Abdessamad Kidari, Murt Redington, Fathima Laffir, Michael J. Pomeroy, Stuart Hampshire

Materials and Surface Science Institute, University of Limerick, Limerick, Ireland

Received 15 July 2010; received in revised form 18 March 2011; accepted 17 April 2011
Available online 18 May 2011

Abstract

Previous work has shown that some RE-Si–Al–O–N glasses are coloured. In particular, oxynitride glasses containing Ytterbium were observed to display a wide range of colours depending on their composition. The reasons for this were not immediately evident. As Ytterbium and Europium have been reported to display valency variations in silicate glasses and α-SiAlONs, the current study prepared a range of Yb–Si–Al–O–N glasses, characterised them by means of X-ray photoelectron, Raman, FTIR and UV–vis spectroscopy as well as thermal analysis and X-ray diffraction. The correlation between the structural features of the glasses with the changes in colour occurring when varying the Yb:Al ratio were investigated. Ytterbium garnet was found to be the source of colour change in the Yb–Si–Al–O–N in the compositions studied.

Keywords: Glass; SiAlON; Colour; Spectroscopy; X-ray methods

1. Introduction

Oxide glasses doped with rare earth ions have been found to have many useful applications, e.g. as optical amplifiers, in lasers and they can also have anti-glare applications. SiO_2 has many desirable properties due to its high transparency, a low coefficient of thermal expansion and good chemical durability. When doped with rare earth ions, SiO_2 can have light absorption in the visible light range.

Ytterbium oxide (Yb_2O_3), a high density oxide, 9.2 g cm^{-3}, has the highest melting point, 2435 °C, among the rare-earth oxides. Its use as a sintering aid for silicon nitride has been investigated.[1] It was found[2] that the Yb–Si–Al–O–N glass had the best oxidation resistance of the Ln–Si–Al–O–N glasses. Various research groups have reported on different crystalline phases within the system.[3–10]

It is reported[11] that rare earth ions show colours due to electron transitions involving the 4f orbitals. The 4f electrons are well shielded beneath an outer electron configuration ($5s^25p^26s^2$) and so are little influenced by the crystal surroundings. Previous research has indicated that rare-earth stabilising cations existed in a single 3^+ valence state and noted that in fact a change between divalent and trivalent states could be induced in Yb (and Sm) α-SiAlON by varying the sintering atmosphere. This valence state controlled novel optical/electrical properties which could extend the field of application of rare-earth doped SiAlONs. It has also been reported[12] that the valence state for Yb in α′ varies (2^+ or 3^+) and is responsible for colouration and may also "influence substitution levels via ionic radii reduction".[13] Optical absorption measurements were made on pressureless sintered samples and hot-pressed samples of the same composition. The hot-pressed samples were a typical black/grey sintered ceramic while the pressureless sintered samples were yellow. Karunaratne et al.[12] attributed this difference to the proximity of the graphite die in the hot press with probable formation of CO gas and hence a reducing atmosphere. Lewis et al.[13] stated that the bright yellow colouration was due to selective absorption of the visible spectrum at short wavelengths.

Uhlig et al.[14] investigated the atomic structure of a range of rare earth glasses with composition (in eq.%) 28Ln:44Si:28Al:85O:15N (Ln = La, Gd, Yb) and found that the Ln–N bonds could not be separated from the Ln–O bonds. Several studies have been dedicated to the effect of lanthanide ions on the properties if Ln–Si–Al–O–N glasses.[15,16] de Graaf

* Corresponding author at: MSG-021, Materials and Surface Science Institute, University of Limerick, Limerick, Ireland. Tel.: +353 61 202821; fax: +353 61 213529.
E-mail address: Wynette.redington@ul.ie (W. Redington).

0955-2219/$ – see front matter © 2011 Elsevier Ltd. All rights reserved.
doi:10.1016/j.jeurceramsoc.2011.04.027

Table 1
Properties for Yb–Si–Al–O–N compositions.

Composition (eq.%)					X-ray diffraction	Colour	Density (g cm^{-3})	Glass transition (°C)	Young's Modulus (GPa)
Yb	Si	Al	O	N					
26	29	45	94	6	Cryst	Green blue	5.1	916.5	216.7
28	28	44	94	6	Cryst	Green blue	5.0	925.9	174.9
28	30	42	94	6	Cryst	Green blue	5.1	–	175.4
28	32	40	94	6	Glass	Yellow	5.2	903.5	214.4
27	27	46	84	16	Cryst	Green blue	5.0	–	–
27	33	40	84	16	Glass	Yellow	5.0	924.4	206.9
27	39	34	84	16	Glass	Yellow	5.1	917.3	165.7

et al.[17] found that Sm- and Yb–Si–Al–O–N glasses show deviations when assuming the trivalent state, indicating mixed oxidation states.

Using such previously published work, as well as results obtained from experimental work,[18] the current paper reports on formation of similar glasses which had measurably different optical properties.

2. Experimental

2.1. Glass preparation

From previously published work, a series of Yb-SiAlON compositions were chosen and these are shown in Table 1. All compositions were calculated as equivalent percent (eq.%). Powder mixtures were produced from high purity oxide and non-oxide powders. The silicon nitride powder used was UBE SN E-10. Yb_2O_3 was 99.9% purity supplied by Stanford Materials, CA. The aluminium oxide was standard Analar grade from Aldrich Chemicals. The silica was quartz powder supplied by Fluka Chemika, Switzerland. AlN was supplied by Aldrich Chemicals. Oxide powders were calcined at 900 °C to remove moisture, chemically absorbed water and volatiles. Once calcined, powders were stored in a dessicator. Nitrides were also kept in a dessicator to reduce the possibility of moisture absorption. In calculating compositions, allowance was made for surface silica on the silicon nitride starting powder. Raw powders were weighed and then mixed into a slurry with isopropanol using a magnetic stirrer. The alcohol was evaporated using a hot plate while being agitated continuously, again using a magnetic stirrer. The dried mixture was sieved through a 0.5 mm aperture sieve to eliminate aggregation. Samples were uni-axially pressed under approximately 150 MPa in a 32 mm diameter steel die to form pellets of 10–15 mm height. The pellets were then packed in a 50:50 (by volume) BN:Si_3N_4 powder bed in an alumina crucible which had been first lined with BN. They were then heated to 1700 °C under 0.1 MPa nitrogen pressure in a graphite resistance furnace at a rate of 10 °C/min. and held for 2 h before furnace cooling at 25 °C/min to room temperature.

Samples were fired in a Carbolite® Lanthanum Chromite vertical tube furnace (serial no. 10/86/1277) heated by lanthanum chromite elements, which stand parallel to the alumina tube axis. Batches of 50 g of powder typically were placed in a graphite mould lined with boron nitride. As the boron nitride powder is inert with respect to the glass composition, wetting of the graphite by the glass melt was prevented. The graphite crucible was placed in the entry port, which was subsequently sealed, evacuated and flooded with 0.1 MPa nitrogen. The sample was then slowly raised into the hot zone at an average heating rate of 50 °C/min to prevent cracking of the alumina insertion tube. It was kept at this temperature for 1 h. A melting temperature of 1700–1715 °C was used in the present work to obtain a homogenous melt. Samples were annealed for 1 h at the glass transition temperature to relieve internal stresses and then slowly cooled to room temperature.

Glass transition temperature, T_g, was determined by DSC (TA Q600) under N_2 and at 10 °C min^{-1} and micrographs of the structure were taken on a Hitachi Su-70 Scanning Electron Microscope. X-ray Diffraction (XRD) was carried out on a Philips X'Pert MPD PRO (40 kV, 35 mA, Cu Kα radiation) to determine whether compositions were amorphous, crystalline, or partly crystalline. Density was measured by an Archimedes method. Elastic modulus was calculated at room temperature from the measurement of the longitudinal, V_l, and transverse, V_t, ultrasonic wave velocities by means of piezoelectric transducers. To determine structure, Raman spectra were collected on mirror polished samples using a Labram DILOR XY (Horiba Jobin Yvon Inc., NJ, USA) using a He–Ne 20 mW, 514.5 nm green source. A grating of 1800 was selected in association with a Peltier cooled CCD detector and the system was coupled to a confocal microscope Olympus model BX40 (×10, ×50 and ×100 objectives). Oxidation state was determined by X-ray Photoelectron Spectroscopy (XPS) performed in a Kratos AXIS 165 spectrometer (Kratos Analytical, Manchester, UK) using monochromatic Al Kα radiation ($h\upsilon$ = 1486.6 eV). Rectangular mirror polished section (15 × 10 × 3 mm) were produced from the melt and fractured under vacuum (~2 × 10^{-8} torr) to create pristine surfaces with minimum contamination. High resolution spectra were taken at pass energy of 20 eV, with step size of 0.05 eV and 100 ms dwell time per step. Surface charging was efficiently neutralised by flooding the surface with low energy electrons. Core level binding energies were corrected using C 1s of adventitious carbon at 284.8 eV as charge reference. For construction and fitting of synthetic peaks of high resolution spectra, a mixed Gaussian–Lorenzian function with a Shirley type background subtraction were used.

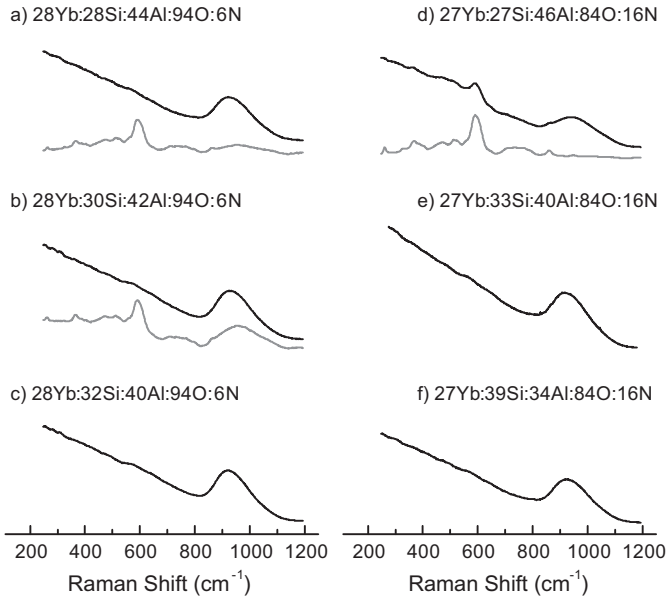

Fig. 1. Raman spectra for the Yb–Si–Al–O–N materials with 6 eq.%N (a), (b) and (c) and 16 eq.% N (d), (e), and (f).

3. Results and discussion

Results of characterisation of properties are given in Table 1. Optical colour as reported was confirmed by FTIR (2500–12000 nm range) and UV–vis (200–800 nm range). The differences in properties between samples that were amorphous and those that were partly crystalline are clear.

The Raman spectra collected with the ×10 objective are shown in Fig. 1. For the materials with the nominal compositions 28Yb:28Si:44Al:94O:6N, 28Yb:30Si:42Al:94O:6N and 27Yb:27Si:46Al:84O:16N (seen in Fig. 1(a), (b) and (d), respectively) it may be noted that different Raman responses were recorded from the samples depending on the region of analysis (crystalline = grey line; glassy = black line). The first type of Raman spectra (grey line) yield sharp features between 200 and 800 cm^{-1} while the second type (black line) were free from the features of the first type as mentioned but had a prominent band between 800 and 1200 cm^{-1}. It must be noted that these latter samples showed $Yb_3Al_5O_{12}$ X-ray reflections. The materials with 28Yb:32Si:40Al:94O:6N, 27Yb:33Si:40Al:84O:16N and 27Yb:39Si:34Al:84O:16N have similar spectra irrespective of the analysed region and showed a single band between 800 and 1200 wavenumbers, see Fig. 1(c), (e) and (f). It can be seen from these results that the sharp features are detected in the partially crystalline materials (grey lines Fig. 1 (a), (b) and (d)) where the crystallinity originates from $Yb_3Al_5O_{12}$. Since the distribution function describing a vibration is a function of the bond angles and lengths, it is wider in appearance in amorphous materials than in crystalline structures. X-ray diffraction analyses indicated that where crystallinity was detected, only the Ytterbium phase occurred. It is therefore reasonable to ascribe these spectra to regions of the samples where the $Yb_3Al_5O_{12}$ is present. Consequently, in $Yb_3Al_5O_{12}$-free regions, in other words, in the fully amorphous regions, samples yield Raman spectra of the second type where a single band between 800 and 1200 cm^{-1} is visible.

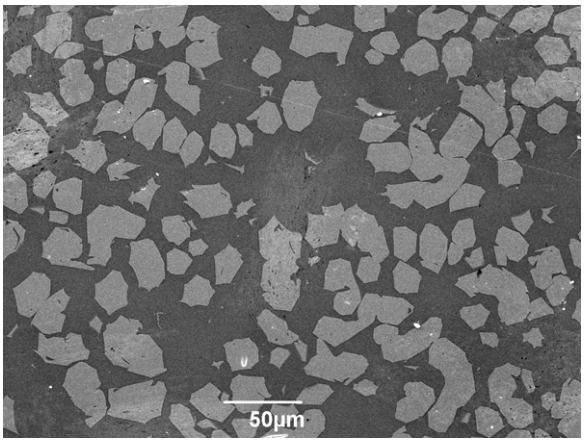

Fig. 2. 28Yb:28Si:44Al:94O:6N (magnification ×1900).

Fig. 2 shows a SEM micrograph for the 28Yb:28Si:44Al:94O:6N material. White irregular-shaped grains (with a grain size ranging from about 10 to 75 μm) are visible amidst a continuous dark matrix. As these features were also identified by the optical microscope attached to the Raman spectrometer, spectra from $Yb_3Al_5O_{12}$ containing materials (28Yb:28Si:44Al:94O:6N, 28Yb:30Si:42Al:94O:6N and 27Yb:46Si:46Al:84O:16N) were recorded using ×100 magnification objective (seen in Fig. 3). The change in objective from ×10 to ×100 was complemented by a decrease in the size of confocal hole from 350 to 190, which effectively reduced the area of the region from which the signal is acquired and thus allowed for more precise acquisition. These selective Raman analyses show (i) that the spectra acquired directly from the white grains alone have sharp peaks, (ii) that measurements carried out on the extended dark region yield a single band between 800 and 1200 cm^{-1} and (iii) that the inter-granular regions give rise to Raman responses that combine the previous indications.

The isolated white areas are therefore identified as $Yb_3Al_5O_{12}$ and the sharp Raman spectra associated with these, confirm their crystalline nature. It is also evident that the black matrix corresponds to the amorphous fraction of the materials. The width and position of the 800–1200 cm^{-1} band is typical of the stretching motion of silicon- to non-bridging oxygen bonds in silicate tetrahedra.[19–21]

Within the intergranular region, the spectra appear as a combination of $Yb_3Al_5O_{12}$ peaks and Si-related stretching motions. Although the laser beam was focused on Yb:YAG free regions, it is likely that scattering occurred from smaller grains or within the bulk of the material. To confirm whether the structure of glass within the inter-granular region differs from that of the bulk, the large band appearing between 800 and 1200 cm^{-1} was decomposed for the spectra of the amorphous and inter-granular regions. Gaussian curves were fitted according to the second derivative of the signal so that the resulting fit was based on observable changes in the signal. Table 2 gives the results of this curve fitting. Despite some variations in the frequency, three

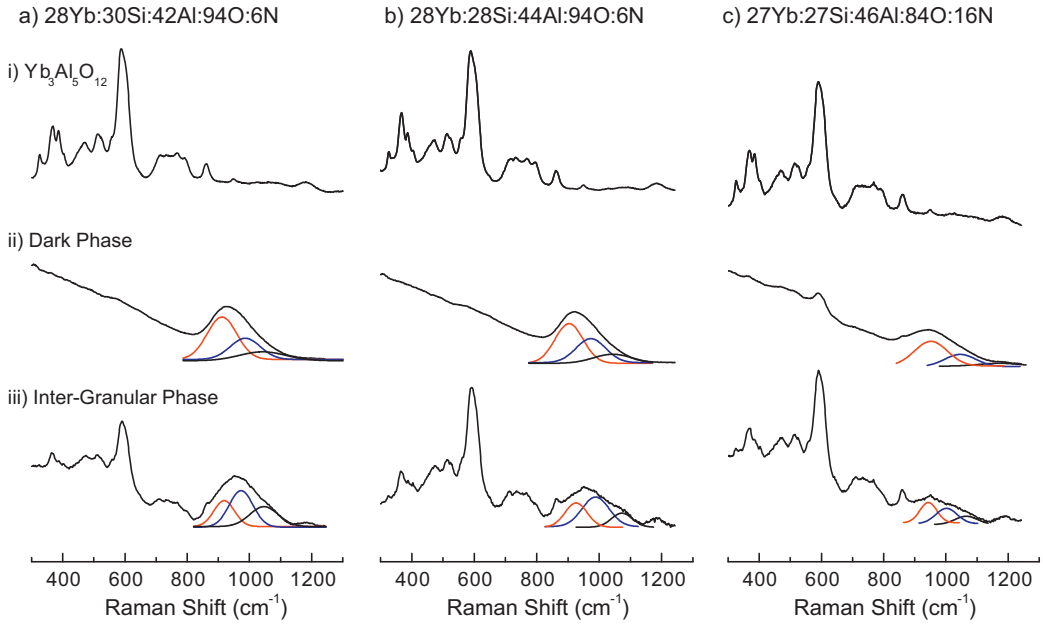

Fig. 3. Gaussian curves fitted to the second derivative of the Raman spectra for the compositions and phases indicated.

bands were systematically fitted—the first one between 900 and 950 cm^{-1}, between 975 and 1050 cm^{-1} for the second and at about 1070 cm^{-1} for the third band. Tabulated data for the area under the fitted components (Table 2) demonstrate that Gaussian curves found between 900 and 950 cm^{-1} for the inter-granular region are smaller than those fitted on the spectra of the bulk glass regions. In contrast to this, the areas of the 975–1050 cm^{-1} and 1070 cm^{-1} bands were higher. It may be concluded that the high frequency components of this band occur at higher concentration around $Yb_3Al_5O_{12}$ grains.

Below 800 cm^{-1}, scattering and fluorescence render spectra of the amorphous regions unusable. Therefore, precise structural assignments have not been considered for these spectra. Nevertheless, the fitting of the high frequency band in both amorphous regions compares well with the assignments made for Si-NBO bonds stretching motion in Q^n silicate tetrahedra (Q^n depicts the number of Si–O–Si bridges per SiO_4 unit): 850 cm^{-1} for Q^0, 900 cm^{-1} for Q^1, 950 and 1000 cm^{-1} for Q^2 and between 1070 and 1170 cm^{-1} for Q^3.[19–21] The 900–950 cm^{-1} bands cover the range for Q^1 and Q^2 silicate structures. The 975–1050 cm^{-1}, i.e. the one reported for Q^2 units and high frequency Gaussian is within the range of Q^3 SiO_4 tetrahedra. These assignments and the data shown in Table 1 offer strong evidence of higher connectivities for the amorphous silicate network around $Yb_3Al_5O_{12}$ grains when compared to the bulk of the samples. There were no significant changes in the numerical values for the fully amorphous materials with 16 eq% N and comparison between crystalline and fully amorphous materials was considered irrelevant because of the structural differences.

Increases in connectivities for the silicate network around $Yb_3Al_5O_{12}$ grains result from fluctuation in the composition when Yb:YAG crystals are precipitated. Writing the reaction describing the precipitation of $Yb_3Al_5O_{12}$ from a given Yb–Si–Al–O–N glass matrix leads to Eqs. (1)–(3) for the 28Yb:28Si:44Al:94O:6N, 28Yb:30Si:42Al:94O:6N and 27Yb:27Si:46Al:84O:N16, respectively:

$$YbSi_{0.8}Al_{1.5}O_{5.04}N_{0.21} \rightarrow \frac{x}{3}(Yb_3Al_5O_{12}) + Yb_{1-x}Si_{0.8}Al_{1.5-5x/3}O_{5.04-4x}N_{0.21} \quad \text{with} \quad x \leq 0.9 \qquad (1)$$

Table 2
Tabulated data for the area under the fitted components.

Composition (eq.%)	Region of analysis	900–950 cm^{-1}	975–1050 cm^{-1}	≈1070 cm^{-1}
27Yb:27Si:46Al:84O:16N	$Yb_3Al_5O_{12}$-free	62	29	9
	Inter-granular	41	38	21
27Yb:33Si:40Al:84O:16N	Fully amorphous	51	30	19
27Yb:39Si:34Al:84O:16N	Fully amorphous	50	35	15
28Yb:28Si:44Al:94O:6N	$Yb_3Al_5O_{12}$-free	48	36	16
	Inter-granular	30	45	25
28Yb:30Si:42Al:94O:6N	$Yb_3Al_5O_{12}$-free	54	28	18
	Inter-granular	27	44	29
28Yb:32Si:40Al:94O:6N	Fully amorphous	51	33	16

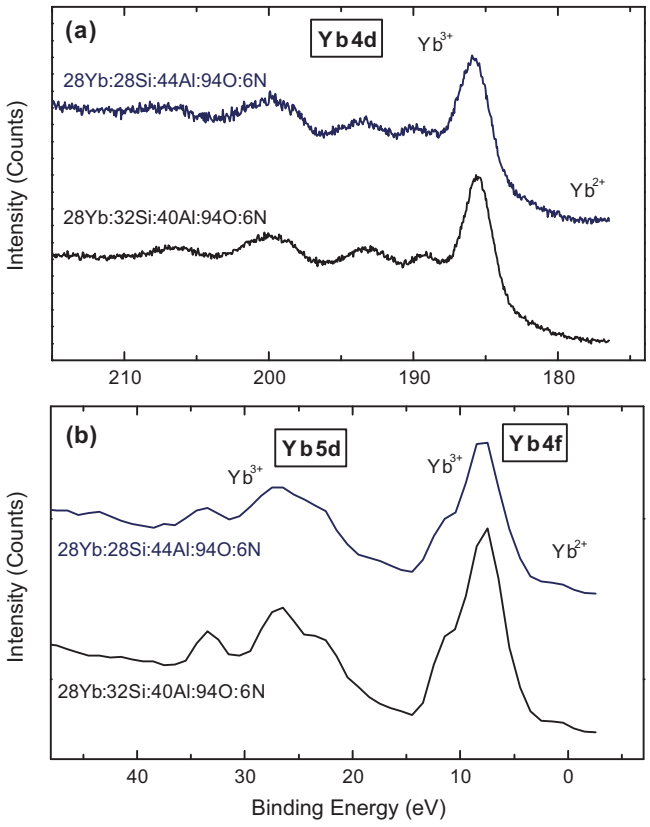

Fig. 4. XPS spectra for 28Yb:28Si:44Al:94O:6N and 28Yb:32Si:40Al:94O:6N.

$$YbSi_{0.75}Al_{1.57}O_{5.04}N_{0.21} \rightarrow \frac{x}{3}(Yb_3Al_5O_{12}) + Yb_{1-x}Si_{0.75}Al_{1.57-5x/3}O_{5.04-4x}N_{0.21} \quad \text{with} \quad x \leq 0.94 \tag{2}$$

$$YbSi_{0.75}Al_{1.7}O_{4.67}N_{0.59} \rightarrow \frac{x}{3}(Yb_3Al_5O_{12}) + Yb_{1-x}Si_{0.75}Al_{1.7-5x/3}O_{4.67-4x}N_{0.59} \quad \text{with} \quad x \leq 1.02 \tag{3}$$

It can be seen that the formation of $Yb_3Al_5O_{12}$ removes Yb, Al and O from the glass matrix and at the same time, renders the glass phase modifier deficient and nitrogen rich. Consequently, it is expected that the inter-granular phase will have a higher connectivity than in the bulk glass from which it originates and the fitting of the 800–1200 cm^{-1} band further supports this.

XPS analysis was carried out to investigate the oxidation state of Yb. The Yb 4d spectra of Yb–Si–Al–O–N materials of the stated compositions are shown in Fig. 4a. Complex structures are seen with the principle peaks appearing at binding energy of 185.5 eV. This is consistent with Yb present in the trivalent state. In addition, the multiplet peaks at 189.1, 192.9, 199.7 and 206.4 eV arising from the $4d^9 4f^{13}$ final states of Yb^{3+} agree very closely with calculations performed by Chorkendorff et al.[22] Similarly, Ohno[24] investigating mixed valence $(YbS)_{1.25}CrS_2$ compound assigned complex multiplet structures of Yb 4d to Yb^{3+}, in addition doublet peaks at 180.3 and 188.8 eV to Yb^{2+}. Peaks corresponding to Yb^{2+} are insignificant in Fig. 4a. The 4f and 5p spectra of the same materials are shown in Fig. 4b. These spectra are dominated by 4f peaks in the range 5–15 eV and 5p doublets deconvoluted at binding energies 27.2 and 33.5 eV which can be characteristically assigned to Yb^{+3}.[23,24] It must be noted there are minor contributions to the peak envelopes from other photoelectron transitions such as O 2s at a binding energy of 23 eV. However, it is evident from spectral positions and intensities that ytterbium as Yb^{3+} dominates in these materials.

4. Conclusions

Different Yb-SiAlON glass compositions have been prepared. Increases in the aluminium content at the expense of silicon lead to devitrification during glass preparation, and Yb:YAG crystals are formed. This structural change triggers a variation in the colour of the materials from brown/yellow in the amorphous state to blue/green when $Yb_3Al_5O_{12}$ precipitates, even at very low levels of crystallinity. Qualitative Raman structural analysis of the glasses and glass–ceramics demonstrate that the connectivity of the silicate network around Yb:YAG grains increases and it is expected that such strengthening occurs when Yb and Al are progressively withdrawn from the glass. Finally, the Yb oxidation state remained constant at 3 for all materials regardless of their composition and structure, devitrification and localised polymerisation do not affect the oxidation state for Yb. Ytterbium garnet is the source of colour changes in Yb–Si–Al–O–N glasses.

Reported work on luminescence of α-SiAlON doped with Ce, Tb, or Eu[25] indicate that there is scope for further study on Yb-glasses for possible optical applications.

Acknowledgements

This work was partly funded by Seed Funding from the Research Office, University of Limerick. The authors wish to acknowledge additional sample preparation and characterisation by Pierre-André Trinsoutrot, ENSIL, Limoges, France.

Appendix A. Supplementary data

Supplementary data associated with this article can be found, in the online version, at doi:10.1016/j.jeurceramsoc.2011.04.027.

References

1. Nishimura T, Mitomo M. Phase relationships in the system Si_3N_4–SiO_2–Yb_2O_3. *J Mater Res* 1995;**10**(2):240–2.
2. Murakami Y, Yamamoto H. Properties of oxynitride glasses in the Ln–Si–Al–O–N Systems (Ln = Rare Earth). *J Ceram Soc Jpn* 1994;**102**:231–6.
3. Cinibulk M, Thomas G, Johnson S. Oxidation behaviour of rare-earth disilicate-silicon nitride ceramics. *J Am Ceram Soc* 1992;**75**(8):2044–9.
4. Hampp E. Phase relationships and sintering behaviour of Yb-doped Si_3N_4. PhD thesis, University of Stuttgart; 1993.

5. Hoffman MJ, Petzow G. Microstructural design of Si_3N_4 based ceramics. *Mater Res Soc Symp Proc* 1993;**287**:3–14.
6. Vetrano JS, Kleebe H-J, Hampp E, Hoffmann MJ, Ruhle M, Cannon RM. Yb-O_3 fluxed sintered silicon nitride. Part I. Microstructure characterisation. *J Mater Sci* 1993;**28**:3529–38.
7. Kanamaru M. Untersuchungen Zur Gefugeentwicklung von Si_3N_4-Keramiken mit Seltenen Eroxiden (Microstructure of silicon nitride densified with rare earth oxides). PhD thesis, University of Stuttgart, Germany; 1994.
8. Nishimura T, Mitomo M, Suematsu H. High temperature strength of silicon nitride ceramics with ytterbium silicon nitride. *J Mater Res* 1997;**12**(1):203–9.
9. Sun W-Y, Tu HY, Wang PL, Yan DS. Nitrogen-rich liquid phase regions in the Ln–Si–Al–O–N (Ln = Nd, Sm, Gd, Dy, Er and Yb) Systems. *J Europ Ceram Soc* 1997;**17**:789–96.
10. Hirosaki N, Yamamoto Y, Nishimura T, Mitomo M, Takahashi J, Yamane H, et al. Phase relationships in the Si_3N_4–SiO_2–Lu_2O_3 system. *J Am Ceram Soc* 2002;**85**(11):861–2863.
11. Judd BD. *Phys Rev* 1962;**127**(3):750.
12. Karunaratne BSB, Lumby RJ, Lewis MH. Rare-earth-doped α-sialon ceramics with novel optical properties. *J Mater Res* 1996;**11**(11):2790–4.
13. Lewis MH, Gajom N, Dobedoe R, Jones AH. Microstructure and property control in SiAlON-containing monolithic and composite ceramics. *Key Eng Mater* 2003;**237**:129–40.
14. Uhlig H, Hoffmann MJ, Lamparter P, Steeb S. Atomic structure of rare earth Si–Al–O–N glasses. *Z Naturforsch A: Phys Sci* 1998;**53**:259–64.
15. Ramesh R, Nestor E, Pomeroy MJ, Hampshire S. Formation of Ln–Si–Al–O–N glasses and their properties. *J Europ Ceram Soc* 1997;**17**:1933–9.
16. Menke Y, Peltier-Baron V, Hampshire S. Effect of rare-earth cations on properties of sialon glasses. *J Non-Cryst Sol* 2000;**276**:145–50.
17. de Graaf D, Le Rol S, Hintzen HT, Le Gendre L, de With G. Mixed oxidation states of Yb and Sm in Si–Al–O–N glasses. *J Eur Ceram Soc* 2006;**26**:2497–501.
18. Redington W. Investigation of liquid and glass forming regions in rare earth SiAlON systems. PhD thesis, University of Limerick; 2003.
19. McMillan P. Structural studies of silicate glasses and melts-applications and limitations of Raman spectroscopy. *Am Miner* 1984;**69**(7–8):622–44.
20. Mysen BO, Virgo D, Kushiro I. The structural role of aluminum in silicate melts—a Raman spectroscopic study at 1 atmosphere. *Am Miner* 1981;**66**(7–8):678–701.
21. McMillan P. A Raman spectroscopic study of glasses in the system CaO–MgO–SiO_2. *Am Miner* 1984;**69**(7–8):645–59.
22. Chorkendorff I, Onsgaard J, Schmidt-May J, Nyholm R. The Yb–Ni interface studied with photoemission spectroscopy. *Surf Sci* 1985;**160**:587.
23. Chung J-S, Cho E-J, Oh S-J. 3d core-level photoemission spectra of intermetallic Yb compounds. *Phys Rev B* 1990;**41**(9):5524–8.
24. Ohno Y. XPS studies of the intermediate valence state of Yb in $(YbS)_{1.25}CrS_2$. *J Elect Spectrosc Related Phenom* 2008;**165**:1–4.
25. Van Krevel JWH, van Rutten JWT, Mandal H, Insten HT, Metselaar R. Luminescence properties of terbium- cerium-, or europium-doped α-sialon materials. *J Solid State Chem* 2002;**165**:19–24.